Chapter 20
Structural Features and Optical Properties of Lithium Niobate Crystals

Nikolay V. Sidorov, Mikhail N. Palatnikov, Natalya A. Teplyakova, Alexander V. Syuy and Dmitry S. Shtarev

Abstract The behavior of the band gap, photorefractive and electroconductive properties depending on the composition, structural features and the defect state of $LiNbO_3$ crystals, nominally pure and doped, obtained both in a single and in different growing technologies, are studied by a set of methods.

20.1 Introduction

Lithium niobate single crystal ($LiNbO_3$) belongs to one of the most important materials of electronic engineering, the physical properties of which can be substantially controlled by its composition [1–3]. The optical homogeneity of crystals is directly related to structural ordering, largely determined by the growing method [4] and relates to one of the fundamental problems of modern materials science. The presence of optical inhomogeneities leads to a change in the physical parameters of the crystals, such as electro-optical coefficients, the refractive index, the absorption coefficient, etc. The presence of optical inhomogeneities in crystals leads to the appearance of regions with biaxiality [5]. All the above deviations of the physical parameters of lithium niobate single crystals lead to incorrect operation of opto-electronic devices, which are made on the base of these crystal. The chemical composition, physico-chemical parameters of the charge and starting materials for the synthesis of charge have a determining effect on the production of crystals with

N. V. Sidorov (✉) · M. N. Palatnikov · N. A. Teplyakova
I.V. Tananaev Institute of Chemistry and Technology of Rare Elements and Mineral Raw Materials of the Kola Science Center of the Russian Academy of Sciences, 26 a, Akademgorodok, Apatity, Murmansk 184209, Russia
e-mail: sidorov@chemy.kolasc.net.ru

A. V. Syuy · D. S. Shtarev
Far Eastern State Transport University, 47, Seryshev Str., Khabarovsk 680021, Russia

D. S. Shtarev
Y.A. Kosygin Institute of Tectonics and Geophysics of Far East Department of Russian Academy of Science, 65, Kim Y. Chen Str., Khabarovsk 680000, Russia

I. A. Parinov et al. (eds.), *Advanced Materials*, Springer Proceedings in Physics 207, https://doi.org/10.1007/978-3-319-78919-4_20

a high degree of structural units, ordering similar to those of stoichiometric composition [6–9]. Fine features of the cation sublattice ordering in lithium niobate crystals are already formed at the stage of charge preparation.

In the lithium niobate crystal, in addition to deep electron traps, created by point photorefractive centers (mainly by Nb_{Li} defects—Nb^{5+} ions, located at Li^{+} ions sites within a perfect structure of stoichiometric composition), there are many small traps that affect the effect of photoinduced change in refractive indices (photorefraction effect, optical damage) and electrical properties [3, 10, 11]. In addition, lithium niobate is a phase of variable composition, which, by doping and variation of stoichiometry, both radically change the properties and subtly control the physical characteristics of the crystal [1, 3]. The number of Nb_{Li} defects and small electron traps depends on the crystal composition [3]. In nominally pure crystals with an increase in the R = Li/Nb ratio, the number of deep electron traps (Nb_{Li} defects) decreases, but at the same time the number of defects in the form of small electron traps increases [3, 12].

When the laser radiation is applied to a ferroelectric $LiNbO_3$ crystal, a spatial separation of the charge occurs as a result of photoexcitation processes (drift and electron diffusion) and an internal electric field arises that leads to a photoinduced change in the refractive indices at the location of the radiation [1, 3, 12, 13]. In the $LiNbO_3$ crystal, the photovoltaic mechanism is the predominant photorefraction mechanism. The value of the photovoltaic field is much larger than the value of the diffusion field [3, 12, 13]. In addition, under the action of laser radiation, Rayleigh photoinduced light scattering (PILS) occurs on static and dynamic (fluctuating) defects with changed refractive index, induced by laser radiation [14, 15]. In this case, the value of the electro-optic effect determines the angle of the PILS indicatrix opening. Photoinduced light scattering in the $LiNbO_3$ crystal occurs predominantly along the polar Z axis [14, 15]. The magnitude and speed of PILS development are determined by the photorefractive sensitivity and speed of photorefractive record of information in electro-optical crystals [15, 16]. The magnitude of the photorefraction effect, photo- and electrical conductivity in the $LiNbO_3$ crystal widely vary depending on the composition [3, 14–22]. In this case, the band gap width must change. The band gap for a nominally pure congruent crystal is 3.72 eV. This is close to the value characteristic for wide-gap semiconductors [13, 16, 23]. By reducing the band gap width, we can approximate the $LiNbO_3$ crystal properties to semiconductor crystals, which allows us to develop materials with cross effects.

In this paper, we have investigated a series of congruent crystals, doped with cations Mg^{2+}(0.35 wt%), Zn^{2+}(2.05), B^{3+}(0.12), Gd^{3+}(0.26, 0.44, 0.51), Y^{3+}(0.46), Gd^{3+}(0.23):Mg^{2+}(0.75), Mg^{2+}(0.86):Fe^{3+}(0.0036), Ta^{5+}(1.13):Mg^{2+}(0.01), Y^{3+}(0.24):Mg^{2+}(0.63), Er^{3+}(3.1), nominally pure stoichiometric lithium niobate crystal ($LiNbO_{3stoich}$). We also studied congruent crystals, grown from a charge, obtained using cyclohexanone $LiNbO_{3cong}$(CHN) as an extractant, as well as from a charge, obtained using cyclohexanone and dimethylamides of carboxylic acids as extractants, $LiNbO_{3cong}$(CHN + DCA).

The investigated crystals have low effect of photorefraction and are promising materials for frequency converters, electro-optical modulators and shutters, optical

materials with micron and submicron periodic structures. Double doping is perspective for obtaining of crystals with increased optical damage resistance.

20.2 Method

Growth of $LiNbO_3$ single crystals was carried out by the Czochralski method in the air atmosphere [7]. The dopant was introduced directly into the melt in the form of the corresponding oxide with impurities less than 10^{-4} wt%. We have used the lithium niobate charge, produced in I.V. Tananaev Institute of Chemistry and Technology of Rare Elements and Mineral Raw Materials of the Kola Science Center of the Russian Academy of Sciences; the technology is described in the work [24]. Stoichiometric crystals were grown from the melt with 58.6 mol% Li_2O. The growth of congruent crystals was made from a charge of a congruent composition (48.6 mol% Li_2O), synthesized from different initial components: niobium pentoxide obtained using cyclohexanone as an extractant (a charge of CHN) and niobium pentoxide obtained using dimethylamides of carboxylic acid (charge CHN + DCA) as an extractant [3, 25]. In the first case ($LiNbO_{3cong}$(CHN) crystals), we have used the CHN charge, and in the second case ($LiNbO_{3cong}$(CHN + DCA) crystals), we have used mixed in a certain proportion CHN charge and CHN + DCA charge. The crystal growing process is described in detail in [3]. Crystalline samples for the studies had the form of rectangular parallelepipeds measuring $\sim 7 \times 6 \times 5$ mm^3 (± 2 mm) with ribs coinciding in direction with the crystal-physical axes *X*, *Y*, *Z*, where the *Z*-axis is the polar axis of the crystal. The edges of the parallelepipeds were thoroughly polished.

The determination of the absorption edge was carried by MDR-41 monochromator. To determine the band gap width, the transmission spectrum of the crystal was recorded. According to the obtained dependence of the intensity of radiation passing through the crystal an inverted spectrum (absorption spectrum) was constructed. The source of radiation was a deuterium lamp. The obtained absorption spectrum in the decreasing linear part of the curve was approximated by a straight line before crossing with the abscissa axis. The intersection point of this line and the abscissa axis is the wavelength corresponding to the absorption edge of the crystal. The width of the band gap was determined by the formulae $E = hc/\lambda$, where λ is the wavelength corresponding to the absorption edge, h is the Planck constant, and c is the speed of light in a vacuum. The error of determining the edge of the absorption edge is ± 1.0 nm.

PILS was excited by a laser Nd:YAG (MLL-100), $\lambda_o = 532$ nm, $I \sim 6.29$ W/cm^2. The scattered radiation falls on a semitransparent screen placed behind the crystal, and is recorded by a digital video camera. The experimental setup and the procedure for determining the PILS indicatrix are described in detail in [15, 26]. In PILS experiments, the laser beam is directed along the *Y*-axis, and the intensity vector **E** of the electric field of the laser radiation is parallel to the polar *Z*-axis of the crystal. The values of the intensities of the photovoltaic and diffusion electric fields, as well as

the induced birefringence in view of the Selmeyer formulae, were determined in the investigated crystals by the parameters of the PILS indicatrix. The installation and methods for determining of the electro-optical coefficients by the interference method and the photoelectric fields are described in detail in the works [27–31]. The error in calculating the photoelectric fields under the experimental conditions is 5–10%. The method of conoscopic studies is described in [32–34]. The laser radiation was used Nd:YAG (MLL-100) (λ_o = 532.0 nm, intensity up to 3.54 W/cm^2). In the PILS experiments and in conoscopic studies, the sample was mounted on a movable two-coordinate optical stage, which made it possible to obtain a number of PILS and conoscopic pictures corresponding to different sections of the sample. The conoscopic picture is recorded on a translucent screen by a digital camera.

The Raman spectra were excited with a 514.5 nm band of the Spectra Physics argon laser (model 2018-RM) and recorded with a Horba Jobin Yvon T64000 spectrograph using a confocal microscope. In this case, Raman spectra were excited by low-power radiation ($P < 3$ mW) to exclude the effect of the photorefraction effect on the spectrum. All spectra are recorded at a resolution of 1.0 cm^{-1} at room temperature. Spectra processing is performed using the Horiba LabSpec 5.0 and Origin 8.1 software package. The error of determining the frequencies, widths and band intensities is ±1.0, ±3.0 cm^{-1} and 5%, respectively.

20.3 Result and Discussion

Table 20.1 demonstrates the results of calculating the band gap width from the absorption spectra of $LiNbO_3$ crystals of different compositions, the values of the photoelectric fields (photovoltaic $\mathbf{E}_{PV}$ and diffusion $\mathbf{E}_D$), and the angle of the PILS indicatrix. In the series of studied crystals the photoelectric fields and the effect of photorefraction (induced birefringence) are minimal for crystals $LiNbO_3$:Er(3.1 wt%), $LiNbO_3$:Gd(0.23 wt%):Mg(0.75), $LiNbO_3$:Y(0.46 wt%), lithium niobate crystal of stoichiometric composition ($LiNbO_{3stoich}$) and maximal for crystal $LiNbO_3$:Mg (0.35 wt%) (Table 20.1). Note that the photoelectric fields and the magnitude of the induced birefringence were determined taking into account the geometric dimensions of the crystals, their orientation in the optical scheme and at the same value of the scattered radiation angle ~6°. We took into account that most of the crystals under study had a clearly reduced photorefraction effect and the largest angle of PILS indicatrix deviation hardly reached 15°. Only in the $LiNbO_{3stoich}$ crystal, the angle of PILS indicatrix reached 56°, with the maximum photovoltaic field ~7.5 kV/cm.

It can be seen from the obtained data that the band gap width for the studied crystals is in the range 3.25–3.84 eV. Crystals of $LiNbO_3$:B(0.12 wt%), $LiNbO_3$:Gd(0.26 wt%) have the smallest width of the band gap as well as crystals with double doping $LiNbO_3$:Fe(0.0036 wt%):Mg(0.86), $LiNbO_3$:Ta(1.13 wt%):Mg (0.011), Table 20.1. Crystals $LiNbO_3$:Gd(0.23 wt%):Mg(0.75) and $LiNbO_3$:Zn

Table 20.1 Photoelectric parameters of the PILS and the of band gap width of lithium niobate crystals at t = 25 °C

Crystal	λ_g (nm)	ΔE_g (eV)	λ = 532 nm, $I \sim$ 6.29 W/cm^2		
			E_{pv} (V/cm)	E_D (V/cm)	$\Delta n\ 10^{-5}$
[a]$LiNbO_3$:Gd(0.23 wt%):Mg (0.75)	323.8	3.84 ± 0.012	3800	745	5.3
[a]$LiNbO_3$:Zn(2.05 wt%)	323.0	3.83 ± 0.012	4770	75	5.6
[a]$LiNbO_{3cong}$	334.2	3.72 ± 0.011	5620	104	6.7
[a]$LiNbO_3$:Er(3.1wt%)	335.2	3.71 ± 0.011	4400	81	5.2
[a]$LiNbO_3$:Mg(0.35 wt%)	341.0	3.65 ± 0.011	7405	295	9.0
$LiNbO_3$:Y(0.24 wt%):Mg (0.63)	342.2	3.63 ± 0.011	5440	98	6.5
$LiNbO_3$:Y(0.46 wt%)	346.4	3.59 ± 0.01	4340	237	5.3
$LiNbO_{3stoich}$	360.0	3.48 ± 0.01	3178	1360	5.3
$LiNbO_3$:B(0.12 wt%)	380.0	3.27 ± 0.009	5374	99	6.4
[a]$LiNbO_3$:Gd(0.26 wt%)	380.0	3.27 ± 0.009	–	–	–
[a]$LiNbO_3$:Fe(0.0036 wt%): Mg(0.86)	382.4	3.25 ± 0.009	4655	127	5.6
$LiNbO_3$:Ta(1.13 wt%):Mg (0.01)	380.0	3.27 ± 0.009	6052	115	7.1

[a]For these crystals the PILS indicatrix does not develop at $I \sim$ 6.29 W/cm^2

(2.05 wt%) have the greatest width, Table 20.1. In the congruent crystal ($LiNbO_{3cong}$), the width of the band gap is close to the maximum (3.72 eV). In this case, the electrical conductivity of a congruent crystal is $\approx 10^{-16}$–10^{-15} $(\Omega \cdot cm)^{-1}$ [35, 36], the conductivity in the directions along the polar Z-axis is much lower than the conductivity perpendicular to the axis [35, 36]. The stoichiometric crystal, according to our data, is characterized by an average value of the band gap width (3.48 eV). Data on the electrical conductivity of the stoichiometric crystal were not found by us. Thus, the composition of the lithium niobate crystal, which affects the features of its secondary structure [3, 10], significantly affects the width of the band gap, the electrical conductivity and the photoelectric fields. Note that for weakly colored crystals $LiNbO_3$:Fe(0.0036 wt%):Mg(0.86) and $LiNbO_3$:Er(3.1 wt%), the absorption bands of the doping element can influence the absorption bands of the crystal [37–39]. Moreover, the closer the corresponding absorption bands to the edge of fundamental absorption is, the stronger is this influence.

Thus, for the studied crystals, a correlation is observed in the values of the band gap, the magnitude of the photoelectric fields, the magnitudes and time dependence of the PILS parameters, the type of conoscopic figures and Raman spectra, Figs. 20.1 and 20.2; Tables 20.1 and 20.2. The defects with electrons, localized on them, are responsible for effect of photorefraction in a $LiNbO_3$ crystal. The main defects in a nominally pure crystal are Nb^{5+} cations, located at the sites of Li^+ cations in a perfect structure (Nb_{Li}), and defects in the form of shallow electron

traps [3, 10–13]. Moreover, the greater the value of R = Li/Nb is, the less the Nb_{Li} defects present in the crystal, but the more defects in the form of shallow electron traps present in the crystal [3, 10, 12]. From the data obtained, it is also seen that the higher photoelectric fields are created in the crystal, the greater the effect of photorefraction is and the farther the PILS indicatrix stretches. At the same time, the induced birefringence increases, this manifests in conoscopic figures.

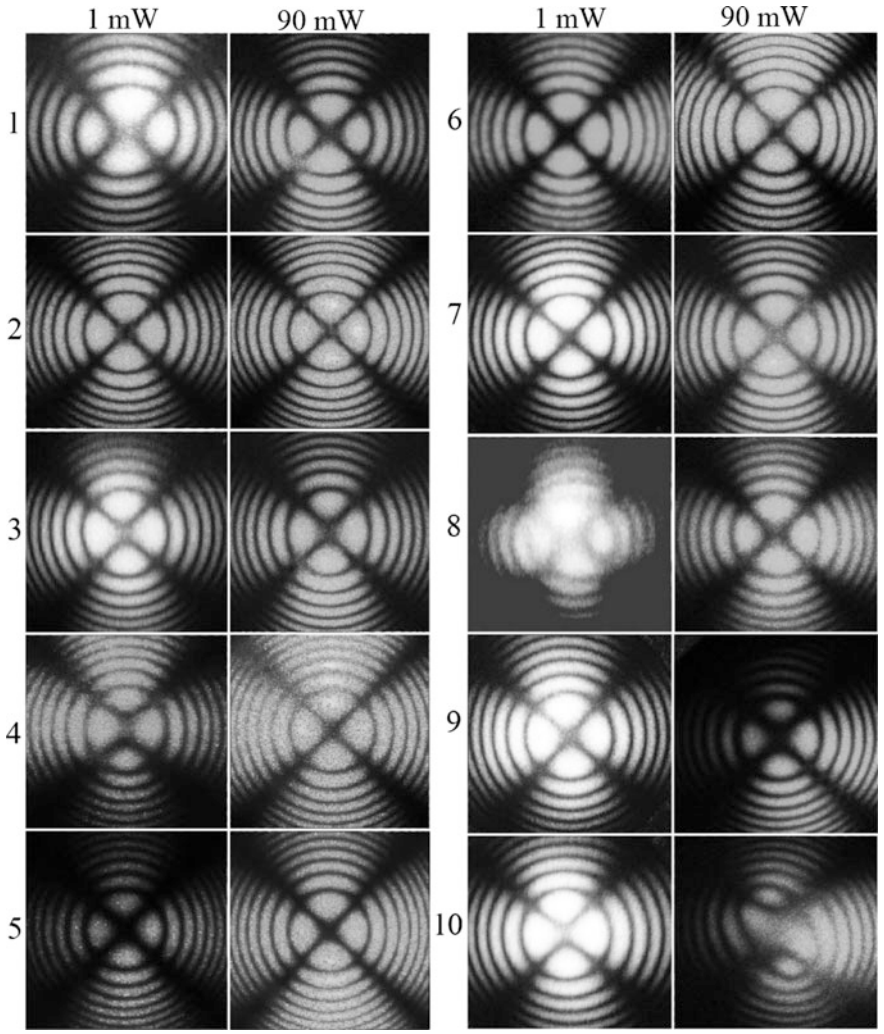

Fig. 20.1 Conoscopic figures of lithium niobate crystals, power of laser radiation: ~1 mW (**a**); ~90 mW (**b**): 1. $LiNbO_3$:Gd(0.51 wt%), 2. $LiNbO_3$:Mg(0.35 wt%), 3. $LiNbO_3$:Gd(0.23 wt%):Mg(0.75), 4. $LiNbO_3$:Zn(2.05 wt%), 5. $LiNbO_3$:Er(3.1 wt%), 6. $LiNbO_3$:Fe(0.0036 wt%):Mg(0.86). 7. $LiNbO_3$:B(0.12 wt%), 8. $LiNbO_3$:Ta(1.13 wt%):Mg(0.011), 9. $LiNbO_3$:Y(0.46 wt%), 10. $LiNbO_3$:Y(0.24 wt%):Mg(0.63)

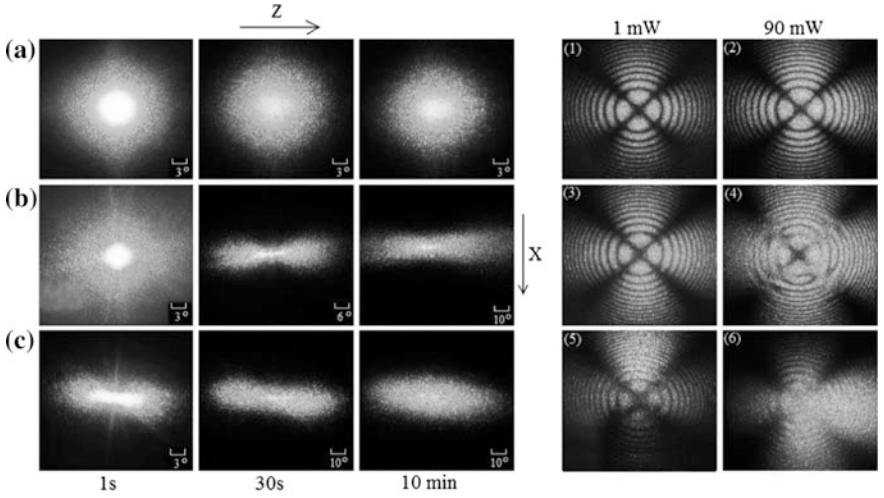

Fig. 20.2 PILS figures of crystals: **a** $LiNbO_{3cong}$(CHN); **b** $LiNbO_{3cong}$(CHN + DCA); **c** $LiNbO_{3stoich}$. λ_0 = 532 nm, I = 6.29 W/cm^2; conoscopic figures of crystals: (1), (2) $LiNbO_{3cong}$(CHN); (3), (4) $LiNbO_{3cong}$(CHN + DCA); (5), (6) $LiNbO_{3stoich}$; λ_0 = 532 nm, I = 0.039 and 3.54 W/cm^2

Figures 20.1 and 20.2 demonstrate conoscopic figures of the studied crystals. When the crystals are irradiated with 1 mW radiation, the conoscopic figures reflect the state of structural defectiveness of the crystal (determined by the composition and crystal growing conditions) in the absence of the photorefraction effect. When laser radiation of power P = 90 mW (λ = 532 nm, d = 1.8 mm) excites conoscopic figures, defects, induced by laser radiation is additionally manifested.

On conoscopic figures of crystals $LiNbO_{3cong}$, $LiNbO_3$:Gd(0.51 wt%), $LiNbO_3$:Mg(0.35 wt%), $LiNbO_3$:Gd(0.23 wt%):Mg(0.75), $LiNbO_3$:Zn(2.05 wt%), $LiNbO_3$:Er(3.1 wt%), $LiNbO_3$:Fe(0.0036 wt%):Mg(0.86), excited by laser radiation of 90 mW, no additional distortions were observed, in comparison with the conoscopic figures obtained at the radiation power of 1 mW (λ = 532 nm, d = 1.8 mm), Figs. 20.1(1–6) and 20.2(1, 2). For these crystals, there was no disclosure of the PILS indicatrix, Table 20.1.

Conoscopic figures of $LiNbO_{3cong}$ crystals, as well as $LiNbO_3$:Mg(0.35 wt%), $LiNbO_3$:Er(3.1 wt%), Figs. 20.1(2, 5) and 20.2(1, 2) correspond to practically perfect conoscopic figures of a uniaxial optically inactive crystal. It is type of figures, which testify the optical homogeneity of the samples and a good optical quality.

Conoscopic figures of lithium niobate crystals $LiNbO_3$:Gd(0.51 wt%), $LiNbO_3$:Gd(0.23 wt%):Mg(0.75), $LiNbO_3$:Zn(2.05 wt%), $LiNbO_3$:Ta(1.13 wt%):Mg(0.011), $LiNbO_3$:Y(0.24 wt%):Mg(0.63), Fig. 20.1(1, 3, 4, 8, 10) contain typical features of biaxial crystals, namely deformation of isochromes and “Maltese cross” with its clarification and rupture into two parts in the center of the field of view.

Table 20.2 The frequencies (ν) and widths (*S*) of the bands in the Raman spectra of single crystals $LiNbO_3$ of different compositions in scattering geometries $Y(ZZ)\overline{Y}(A_1(TO))$ and $Y(ZX)\overline{Y}(E(TO))$ at t = 25 °C

$LiNbO_{3stoich}$		$LiNbO_{3cong}$		$LiNbO_3$:Zn (2.05 wt%)		$LiNbO_3$:B (0.12 wt%)		$LiNbO_3$:Y (0.24):Mg (0.63 wt%)		$LiNbO_3$:Y (0.46 wt%)		$LiNbO_3$:Gd (0.44 wt%)	
ν	*S*	ν	*S*	ν	*S*	ν	*S*	ν	*S*	ν	*S*	ν	*S*
A_1(TO)													
253	21	252	30	259	24	255	24	251	32	254	30	252	32
277	11	276	12	280	16	277	14	275	13	273	14	275	13
333	8	332	10	335	14	333	11	331	10	330	12	331	9
632	20	631	25	624	31	629	23	631	26	632	29	632	26
E(TO)													
156	7	156	12	154	16	155	9	151	11	152	12	148	11
240	9	240	11	238	16	240	10	236	11	237	12	234	11
268	10	268	14	266	32	270	13	264	12	264	14	261	14
324	10	324	13	326	18	324	14	321	15	322	20	318	15
371	17	371	23	371	30	370	26	368	24	368	28	365	24
434	10	434	14	437	15	432	11	432	14	434	16	429	12
576	16	576	15	579	31	576	33	578	22	578	27	576	23
632[a]	31	626	25	631	35	626	46	616	83	622	95	627	50

[a]band with frequency ~630 cm^{-1}; A_1(TO) is appeared in the Raman spectrum in the scattering geometry $Y(ZX)\overline{Y}$, in which E(TO) phonons are active, due to the effect of photorefraction

In this case, the isochromes have the form of ellipses. The "Maltese Cross" is divided into two parts with their shift in the direction from the center, corresponding to the direction of deformation of the optical indicatrix of the crystal. When the laser radiation power is increased to 90 mW, the signs of anomalous optical biaxiality on crystal conoscopic figures $LiNbO_3$:Gd(0.51 wt%), $LiNbO_3$:Zn(2.05 wt %) and $LiNbO_3$:Ta(1.13 wt%):Mg(0.011), Fig. 20.1(1, 4, 8) decrease. The conoscopic figures of these crystals become less deformed, which is obviously related to the "healing" of defects in crystals by the laser radiation.

On the conoscopic figures of crystals $LiNbO_{3stoich}$, $LiNbO_3$:B(0.12 wt%), $LiNbO_3$:Ta(1.13 wt%):Mg(0.011), $LiNbO_3$:Y(0.46 wt%), $LiNbO_3$:Y(0.24 wt%):Mg(0.63), for which the PILS indicatrix was revealed, Table 20.1, with an increase in the laser radiation power up to 90 mW, additional anomalies appear that are absent in the conoscopic figures at 1 mW. It is obviously associated with the appearance of defects induced by laser radiation in the crystal structure. Especially strong deformation of conoscopic figures with increasing in laser radiation power is characteristic for crystals $LiNbO_{3stoich}$ and $LiNbO_3$:Y(0.24 wt%):Mg(0.63), Figs. 20.1(10) and 20.2(6) for which a rapid disclosure of the PILS indicatrix is characteristic, Table 20.1. The appearance of an anomalous optical biaxiality with increasing in the laser radiation power is probably connected with the existence of local regions in a crystal with birefringence.

For crystals $LiNbO_{3cong}$, $LiNbO_3$:Gd(0.51 wt%), $LiNbO_3$:Mg(0.35 wt%), $LiNbO_3$:Gd(0.23 wt%):Mg(0.75), $LiNbO_3$:Zn(2.05 wt%) even at a relatively high intensity of the exciting radiation ($I \sim 6.29$ W/cm^2) photorefractive response is absent, the PILS indicatrix is not revealed, but only circular scattering is observed on static structural defects. The scattering figure does not change in time and retains a shape close to the circle throughout the experiment. At the same time for crystals $LiNbO_{3stoich}$, $LiNbO_3$:B(0.12 wt%), $LiNbO_3$:Ta(1.13 wt%):Mg(0.011), $LiNbO_3$:Y (0.46 wt%), $LiNbO_3$:Y(0.24 wt%):Mg(0.63) a photorefractive response is characteristic of crystals, Table 20.1, and the disclosure of the PILS indicatrix is observed with the appearance of a pronounced three-layered speckle structure that significantly changes over time. In this case, energy is transferred from the central region of the PILS figure (the region of the laser beam incidence) to the scattered radiation. For crystals $LiNbO_{3stoich}$, $LiNbO_3$:B(0.12 wt%), $LiNbO_3$:Ta(1.13 wt%):Mg(0.011), PILS images opened for $\sim$60 s, and they transform with time into an oval ("comet") shape from the round shape (first seconds of excitation), and then take the form of an asymmetric "eight" oriented along the polar axis of the crystal. In the positive direction of the polar axis, coinciding with the direction of the spontaneous polarization vector, a larger "petal" of the figure "eight" develops, and in the negative direction, the smaller one. For this group of crystals, the gradual transfer of energy of different layers of the PILS figure in the direction of the polar axis of the crystal is also characteristic over time. For crystals $LiNbO_3$:Y(0.46 wt%) and $LiNbO_3$:Y(0.24 wt%):Mg(0.63), the disclosure of the PILS indicatrix is much faster than the rest of the crystals during the first second of irradiation of the crystal by laser radiation. It is noteworthy that for crystals $LiNbO_{3stoich}$, $LiNbO_3$:B(0.12 wt%), $LiNbO_3$:Ta(1.13 wt%):Mg(0.011), $LiNbO_3$:Y(0.46 wt%), $LiNbO_3$:Y(0.24 wt%):

Mg(0.63), difference is less in comparison with other crystals, the band gap width, the strongest photorefractive response is observed and the PILS indicatrix reveals the greatest opening, Table 20.1.

Table 20.2 shows the values of some Raman bands widths of crystals $LiNbO_{3stoich}$, $LiNbO_{3cong}$, $LiNbO_3$:B(0.12 wt%), $LiNbO_3$:Y(0.46 wt%), $LiNbO_3$:Y (0.24 wt%):Mg(0.63), $LiNbO_3$:Gd(0.44 wt%), $LiNbO_3$:Zn(2.05 wt%), corresponding to fundamental vibrations A_1(TO) and E(TO) type symmetry, occurring, respectively, along and perpendicular to the polar axis of the crystal. It can be seen that the smallest values of the width of the majority of bands have the Raman spectrum of crystals $LiNbO_{3stoich}$ and $LiNbO_3$:B(0.12 wt%), and the largest values for the spectrum of the crystal $LiNbO_3$:Zn(2.05 wt%). Moreover, the strongest dependences of the widths on the crystal composition are characteristic for bands with frequencies 630 A_1(TO) and 576 cm^{-1} (E(TO)), corresponding, respectively, to the completely symmetric and doubly degenerate vibrations of the oxygen atoms of the octahedra O_6. Unusual is that the band with frequency 576 cm^{-1} has the largest width in the spectrum of the crystal $LiNbO_3$:B(0.12 wt%), in comparison with other studied crystals, Table 20.2. This can be explained by the fact that non-metallic cations B^{3+} practically do not enter the structure of the crystal $LiNbO_3$, but they structure the melt, thus affecting the structural features and optical properties of the crystal. With a content of about 1.2 mol% B_2O_3 in the melt, in the crystal there will be only $\sim 4 \times 10^{-4}$ mol% B_2O_3, which corresponds to the concentration of uncontrolled trace of numerous cationic impurities in the crystal $LiNbO_3$ (Zr, Mo, Ca, Fe, Ti, Si et al.) [7–9, 24].

According to the Raman tensor in the spectrum in the scattering geometry $Y(ZX)\overline{Y}$, only bands, corresponding to oscillations of the E (TO) type of symmetry, should be present [3]. However, in the Raman spectra of all the studied crystals, owing to the presence of the photorefraction effect, there is a band with frequency ~ 630 cm^{-1}, which corresponds to the totally symmetric vibrations of oxygen octahedra of the A_1 type of symmetry. By measuring the intensity of the "forbidden" band with frequency 630 cm^{-1}, it is possible to estimate the magnitude of the photorefractive effect [3]. At the same time, the width of this band, as well as the band width with frequency 576 cm^{-1} (E(TO)), indicates a degree of distortion of oxygen octahedra O_6. Table 20.2 shows that the minimum band width with frequency ~ 630 cm^{-1} is observed for a crystal $LiNbO_{3stoich}$, characterized by the most ordered cation sublattice, but a high photorefraction effect. Band width with frequency ~ 630 cm^{-1} in the spectrum of crystals $LiNbO_{3stoich}$, $LiNbO_3$:B(0.12 wt%), $LiNbO_3$:Y(0.46 wt%), $LiNbO_3$:Y(0.24 wt%):Mg(0.63), for which there was a disclosure of the PILS indicatrix, Table 20.1, increases, in comparison with the width in the spectrum of the crystal $LiNbO_{3cong}$, Table 20.2. However, the increase in width occurs not in proportion to the increase in the opening angle of the PILS indicatrix, Tables 20.1 and 20.2. The greatest angle of disclosure of the PILS indicatrix is observed for a crystal $LiNbO_{3stoich}$, Table 20.1, and the largest band width with frequency ~ 630 cm^{-1} for crystal $LiNbO_3$:Y(0.46 wt%), Table 20.2. In addition, the width of this band in the Raman spectrum of crystals $LiNbO_3$:Gd(0.44 wt%) and

$LiNbO_3$:Zn(2.05 wt%) is broader than in the spectrum of the crystal $LiNbO_{3stoich}$, Table 20.2. This is because the contribution to the width of the band with frequency $\sim 630\ cm^{-1}$ is brought not only by the effect of photorefraction, but also by the degree of distortion of the oxygen octahedra of the crystal, which depends on the composition. The distortion of oxygen octahedra is influenced, first of all, by differences in the ionic radii of the doping cations and ions Li^+, Nb^{5+}, the nature of the bonds, formed by cations with oxygen ions, as well as the particular order in the location of the basic and doping cations and vacancies along the polar axis.

Usually single crystals of congruent composition (R = Li/Nb = 0.946) are applied. At the same time, for the production of materials with submicron periodically polarized domain structures, perfected lithium niobate single crystals of stoichiometric composition (Li/Nb = 1) have a significant advantage in comparison with congruent crystals because they have a significantly lower (five times or more) coercive field [6]. However, stoichiometric crystals grown from a melt with 58.6 mol% Li_2O are characterized by a high inhomogeneity of the refractive index along the growth axis, and also, much higher than the congruent crystal effect of photorefraction (optical damage) [3, 6, 12, 26, 40]. In addition, the considerable heterogeneity of the composition along the length of the monocrystal, arising during the growth process, makes it difficult to grow stoichiometric crystals of sufficiently large size [1, 3], suitable for industrial manufacturing of optical elements. Congruent single crystals have a high constancy of the refractive index along the growth axis [1, 3].

Figure 20.2 demonstrates PILS figures and conoscopic pictures of a stoichiometric single crystal $LiNbO_{3stoich}$ and congruent single crystals grown from a charge of various geneses. Single crystals of congruent composition are grown from a charge, obtained using cyclohexanone as an extractant — $LiNbO_{3cong}$(CHN), as well as from the charge, obtained using cyclohexanone and dimethylamides of carboxylic acids as extractants — $LiNbO_{3cong}$(CHN + DCA) [3]. Laser conoscopy methods and PILS do not give direct information about the features of the internal structure of crystals and defects that determine their photorefractive properties, but they allow obtaining preliminary information on optical homogeneity and photorefractive properties of crystals, which is important at the stage of development of technology for growing lithium niobate crystals.

PILS, arising on spatial microdefects with a laser (static) or fluctuating refractive index, changed under the influence of laser radiation, causes a strong destruction of the laser beam in the crystal and is an interfering factor for the generation and transformation of radiation [14, 15]. The shape and features of the speckle structure of the PILS indicatrix depend on the features of the structure of the crystal, the state of its defectiveness, and also on the polarization of the radiation and the geometry of the experiment [14, 15].

For crystal $LiNbO_{3cong}$(CHN) even after irradiation for 10 min by laser radiation with a power density 6.29 W/cm^2, the PILS indicatrix is not disclosed, but only circular scattering is observed on static structural defects, Fig. 20.2a. It should be noted that the central layer of the speckle structure of the crystal $LiNbO_{3cong}$(CHN)

PILS, Fig. 20.2a, corresponding to the cross-section of the laser beam, disappears almost completely within the first 30 s after the beginning of the irradiation of the crystal, then reappears.

At the same time, crystals $LiNbO_{3cong}$(CHN + DCA) and $LiNbO_{3stoich}$ PILS figures vary considerably over time, Fig. 20.2b, c. Indicatrix of PILS froms a rounded shape with time is transformed first into an oval ("comet") shape, and then takes the form of an asymmetric "eight", oriented along the polar axis of the crystal. For these crystals, the gradual shift of the intensity of different layers of the PILS figure in the direction of the polar axis of the crystal is also characteristic over time, Fig. 20.2b, c. For the crystal $LiNbO_{3stoich}$ indicatrix of PILS is revealed in the first seconds of irradiation, Fig. 20.2c. The opening angle of the PILS is 66° and 56° for crystals $LiNbO_{3cong}$(CHN + DCA) and $LiNbO_{3stoich}$, respectively.

Often a congruent charge of lithium niobate [3] leads to appearance of a slightly greenish or yellowish-greenish color in single crystals. The presence of the color can limit the possibility of single crystals application for optical devices that require optical perfection of the material. The appearance of color is due to the appearance in the crystal of cluster defects in the form of molecular complexes on the base of intrinsic and impurity defectiveness. This defectiveness is partly laid down at the stage of preparation of the initial niobium pentoxide by extraction [3]. It is possible to obtain perfectly colorless (water white) $LiNbO_3$ crystals using a mixture of charge synthesized from niobium pentaoxides produced with the help of different extractants: carboxylic acid amides and cyclohexanone. Apparently, the use of lithium niobate charge, mixed in a certain proportion of different genesis, leads to compensation of defect formation mechanisms and to the absence of visible color of the crystal. Comparative studies of crystals, grown from one type of charge,—$LiNbO_{3cong}$ (CHN) and from the mixture—$LiNbO_{3cong}$(CHN + DCA) showed significantly higher optical homogeneity, as well as an absolute visual colorlessness (water white) in crystals, grown from a mixture of charge, synthesized from niobium pentaoxides, produced by various extractants [3]. In addition, for the crystal $LiNbO_{3cong}$(CHN + DCA) the fundamental absorption edge is essentially shifted to the region of short wavelengths in comparison with the crystal $LiNbO_{3cong}$(CHN) [41], which means it has a substantially larger optical transparency window. The latter indicates a higher degree of structural perfection of congruent crystals $LiNbO_{3cong}$(CHN + DCA), apparently, approaching the degree of structural perfection of crystals of stoichiometric composition $LiNbO_{3stoich}$.

It was established in [14] that small electronic traps can form in structurally imperfect lithium niobate crystals. In such crystals, the contribution of the energy of the electronic subsystem to the total energy of the crystal is high [23]. At the same time, the photorefractive effect is noticeably reduced due to an increase in the efficiency of the eradicative recombination of photo-excited carriers without their capture to deep levels. The reasons for this are that when the crystal is illuminated by the laser radiation, there are two competing processes. On the one hand, with an increase in the degree of structural perfection in the crystal, the number of charged defects and associated deep trapping levels in the band gap decreases, on the other hand, the number of small traps ("sticking levels" [14]) decreases and, accordingly,

decreases the probability of eradicative recombination photoexcited carriers. The main part of the photoelectrons is captured by the existing deep traps. Consequently, uncompensated internal electric fields that affect the refractive index and determine the photorefractive properties of the crystal become larger. This, apparently, explains the greater effect of photorefraction in more structurally perfect crystals $LiNbO_{3stoich}$ and $LiNbO_{3cong}$(CHN + DCA) in comparison with the crystal $LiNbO_{3cong}$(CHN), Fig. 20.2.

The optical homogeneity of the crystals was investigated by laser conoscopy at laser power densities (I) (λ_o = 532 nm) 0.039 и 3.54 W/cm^2, Fig. 20.2.

For the crystal $LiNbO_{3cong}$(CHN), standard conoscopic pictures of a uniaxial crystal of high optical quality are observed, Fig. 20.2(1, 2). On the background of concentric rings-isochromes, the branches of the "Maltese cross", formed by two isogyres of minimum intensity, intersect at the center of the field of view, perpendicular to each other and coincide with the transmission axes of the polarizer and analyzer.

Crystal $LiNbO_{3cong}$(CHN + DCA) conoscopic figures at radiation power density 0.039 W/cm^2 have a standard shape, corresponding to a uniaxial crystal, and consist of a contrasting black "Maltese cross", which is superimposed on concentric rings-isochromes, centered at the exit point of the optical axis, coinciding with the center of the "Maltese cross". The "Maltese Cross" retains the minimum intensity within the entire field of view, Fig. 20.2(3). When the power density of the laser radiation is increased to 3.54 W/cm^2 was also obtained a conoscopic figure, corresponding to a uniaxial crystal, Fig. 20.2(4), but it is much more deformed than the conoscopic figure at 0.039 W/cm^2, Fig. 20.2(3). There is a decrease in the contrast and clarity of the image, there is a significant violation of the circular symmetry of the rings-isochromes, there is marked pairing, discontinuities, dislocations and inconsistencies with isochromes, when crossing the "Maltese cross" branches, Fig. 20.2(4). Significant deformation of the conoscopic patterns with increasing laser radiation power density from 0.039 to 3.54 W/cm^2 for the crystal $LiNbO_{3cong}$(CHN + DCA) is probably due to this crystal is characterized by a significant photorefractive response, Fig. 20.2b.

Figure 20.2(5, 6) demonstrates conoscopic patterns of the crystal $LiNbO_{3stoich}$. As with small (0.039 W/cm^2), and with a large (3.54 W/cm^2) power density of laser radiation, the conoscopic patterns are significantly deformed. On both conoscopic crystal figures $LiNbO_{3stoich}$ there are signs of anomalous optical biaxiality, in which there is a deformation of the optical indicatrix of the crystal in the vertical direction, corresponding to the direction of the shift of the "Maltese cross" parts. In this case, the isochromes are stretched in the direction of displacement of the fragments of the cross and take the form of ellipses. Each ring-isochrome, being a line of the same phase shift, corresponds to a cone of rays with the same angle of incidence when the axis of the conical radiation beam coincides with the optical axis of the crystal. Such anomalies of conoscopic figures indicate a significant optical inhomogeneity of the crystal $LiNbO_{3stoich}$. The increase in the power of laser radiation, Fig. 20.2(6), leads to a decrease in the overall contrast and sharpness of the image, as well as to a noticeable "blurring" of the branches of the "Maltese cross". Significant distortion of

conoscopic patterns for a crystal $LiNbO_{3stoich}$, when the power density of the laser radiation is increased to 3.54 W/cm^2 is apparently due to the presence of a significant photorefractive response, Fig. 20.2c.

By the interference method, using the technique described in [27], the electro-optical coefficients are determined, which for a crystal $LiNbO_{3stoich}$ amounted to r_{22} = 6.4 pm/V and $r_e = n_0^3 r_{13} - n_e^3 r_{33}$ = 19.3 pm/V, for a congruent crystal $LiNbO_{3cong}$(CHN + DCA) amounted to r_{22} = 6.5 pm/V and $r_e = n_0^3 r_{13} - n_e^3 r_{33}$ = 29.3 pm/V. According to the literature, r_e for crystal $LiNbO_{3cong}$(CHN) amounted to 17–19 pm/V. Thus, it can be stated that the crystals $LiNbO_{3cong}$(CHN + DCA) have significantly higher electro-optical properties than crystals $LiNbO_{3cong}$(CHN).

20.4 Conclusion

Absorption spectra, Raman spectra and PILS figures were researched for $LiNbO_3$ crystals nominally pure and doped with cations: Mg^{2+}(0.35 wt%), Zn^{2+}(2.05), B^{3+}(0.12), Gd^{3+}(0.26, 0.44, 0.51), Y^{3+}(0.46), Gd^{3+}(0.23):Mg^{2+}(0.75), Mg^{2+}(0.86):Fe^{3+}(0.0036), Ta^{5+}(1.13):Mg^{2+}(0.01), Y^{3+}(0.24):Mg^{2+}(0.63), Er^{3+}(3.1). It is established that the position and character of the behavior of the absorption edge of lithium niobate crystals depends on the type of the dopant. The width of the band gap of crystals is calculated from the parameters of the absorption edge. It is shown that the width of the band gap depends on the state of the defect structure of the crystals, which determines the magnitude of the photorefraction effect. The smaller width of the band gap is observed in crystals $LiNbO_{3stoich}$, $LiNbO_3$:B(0.12), $LiNbO_3$:Ta(1.13):Mg(0.011), $LiNbO_3$:Y(0.46), $LiNbO_3$:Y(0.24):Mg(0.63). In these crystals, a photorefractive response is present and the PILS indicatrix is revealed, when irradiated with laser radiation of λ_0 = 476.5 nm and the radiation intensity $I \sim$ 8.49 W/cm^2. In the crystals $LiNbO_{3stoich}$, $LiNbO_3$:Y(0.46 wt%), $LiNbO_3$:Y(0.24):Mg(0.63), the disclosure of the PILS indicatrix occurs very quickly, during the first second of irradiation of the crystal by laser radiation. In Raman spectra of these crystals, a significant broadening of the bands, corresponding to vibrations of cations, located in octahedral void spaces, and vibrations of the oxygen octahedra of the A_1(TO) and E(TO) symmetry type is revealed, indicating an increased disorder in the structural units of crystals. The optical homogeneity and photorefractive properties of stoichiometric and congruent lithium niobate crystals, grown from the charge of different genesis are investigated. It is shown that for crystals $LiNbO_{3cong}$(CHN) at a power density of laser radiation up to 6.29 W/cm^2 the PILS indicatrix is not disclosed, but only circular scattering is observed on static structural defects. For crystals $LiNbO_{3cong}$(CHN + DCA) and $LiNbO_{3stoich}$ the PILS indicatrix is fully revealed within a minute from the beginning of irradiation with laser radiation, the opening angle is 66° and 56°, respectively. Investigation of optical homogeneity of crystals by laser conoscopy showed a sufficiently high

optical quality of crystals $LiNbO_{3cong}$(CHN) and $LiNbO_{3cong}$(CHN + DCA). On both $LiNbO_{3stoich}$ crystals conoscopic figures, obtained for small (0.039 W/cm^2) and large (3.54 W/cm^2) power density of laser radiation has signs of anomalous optical biaxiality. Crystal $LiNbO_{3cong}$(CHN + DCA) is more optically homogeneous than $LiNbO_{3stoich}$, but at the same time it has a great effect of photorefraction and substantially higher electro-optical properties than the crystal $LiNbO_{3cong}$(CHN).

References

1. Y.S. Kuzminov, *Electro-optical and Nonlinear-optical Lithium Niobate Crystal* (Nauka, Moscow, 1987) (in Russian)
2. G.G. Gurzadyan, V.G. Dmitriev, D.N. Nikogosyan, *Nonlinear Optical Crystals. Properties and Applications in Quantum Electronics* (Radio and Communication, Moscow, 1991) (in Russian)
3. N.V. Sidorov, T.R. Volk, B.N. Mavrin, V.T. Kalinnikov, *Lithium Niobate: Defects, Photorefraction, Vibrational Spectra, Polaritons* (Nauka, Moscow, 2003) (in Russian)
4. S.V. Mikhlyaev, *Mater. Electron. Eng.* (2), 32 (2013)
5. V.V. Krishtop, M.N. Litvinova, V.G. Efremenko, V.I. Stroganov, A.V. Syuy, A.V. Denisov, O.S. Grunsky, Opt. J. **73**(12), 84 (2006)
6. M.N. Palatnikov, N.V. Sidorov, *Oxide Electronics and Functional Properties of Transition Metal Oxides* (NOVA Sience Publishers, New York, 2014), p. 31
7. M.N. Palatnikov, I.V. Biryukova, N.V. Sidorov, A.V. Denisov, V.T. Kalinnikov, P.G.R. Smith, V.Y. Shur, J. Cryst. Growth **291**, 390 (2006)
8. M.N. Palatnikov, I.V. Biryukova, S.M. Masloboeva, O.V. Makarova, D.V. Manukovskaya, N.V. Sidorov, J. Cryst. Growth **386**, 113 (2014)
9. M.N. Palatnikov, S.M. Masloboeva, I.V. Biryukova, O.V. Makarova, N.V. Sidorov, V.V. Efremov, J. Inorg. Chem. **59**(3), 318 (2014)
10. N.V. Sidorov, M.N. Palatnikov, V.T. Kalinnikov, *Influence of the Secondary Structure on Optical Properties of Ferroelectric Crystals of Lithium Niobate with Low Photorefractive Effect.* Proc. KSC RAS. Chemistry and Materials. Apatity (2015) (in Russian)
11. A.A. Blistanov, V.M. Lyubchenko, A.N. Goryunova, Kristallographija **43**(1), 86 (1998)
12. T. Volk, M. Wohlecke, *Lithium Niobate. Defects, Photorefraction and Ferroelectric Switching* (Springer, Berlin, 2008)
13. M. Lines, A. Glass, *Ferroelectrics and Related Materials* (Mir, Moscow, 1981) (in Russian)
14. V.V. Obukhovsky, *Processes of Photorefractive Scattering of Light in Crystals*, Ph.D. Thesis, Kiev, 1989 (in Russian)
15. V.A. Maksimenko, A.V. Syui, Y.M. Karpets, *Photoinduced Processes in Lithium Niobate Crystals* (Fizmatlit, Moscow, 2008) (in Russian)
16. S.G. Odulov, M.S. Soskin, A.I. Khizhnyak, *Lasers on Dynamic Gratings* (Nauka, Moscow, 1990) (in Russian)
17. A.S. Pritulenko, A.V. Yatsenko, S.V. Evdokimov, Kristallographija **60**(2), 293 (2015)
18. A.V. Yatsenko, S.V. Yevdokimov, A.S. Pritulenko, D.Y. Sugak, I.M. Solskii, Phys. Solid State **54**, 2231 (2012)
19. A. Weidenfelder, J. Shi, P. Fielitz, G. Borchardt, K.D. Becker, H. Fritze, Solid State Ion. **225**, 26 (2012)
20. A.A. Bulycheva, *Electrical Conductivity and Electron-hole Processes in Lithium Niobate Crystals Heavily Doped with Magnesium Oxide*, PhD Thesis, Tomsk, 2005 (in Russian)

21. K.K. Wong, *Properties of Lithium Niobate* (INSPEC, The Institution of Engineers, London, 2002)
22. A.A. Blistanov, V.V. Geraskin, A.V. Khretinina, *Izv. High Schools. Mater. Electron. Eng.* (1), 28 (1998)
23. V.M. Fridkin, *Ferroelectrics–Semiconductors* (Nauka, Moscow, 1976) (in Russian)
24. M.N. Palatnikov, N.V. Sidorov, I.V. Biryukova, O.B. Shcherbina, V.T. Kalinnikov, *Perspekt. Mater.* (2), 93 (2011) (in Russian)
25. M.N. Palatnikov, N.V. Sidorov, V.T. Kalinnikov, *Ferroelectrical Solid Solutions Based on Oxyde Compounds of Niobium and Tantalum: Synthesis, Research of Structure Order and Physical Characteristics* (Nauka, Saint-Petersburg, 2001) (in Russian)
26. N.V. Sidorov, E.A. Antonycheva, A.V. Syui, M.N. Palatnikov, Kristallographija **55**(6), 1079 (2010)
27. A.V. Syuy, E.O. Kile, in *Proceedings of SPIE. Aisa-Pacific Conference on Fundamental Problems of Opto- and Microelectronics*, 101761N (2016). https://doi.org/10.1117/12.2268233
28. M. Goulkov, M. Imlau, Th Woike, Phys. Rev. **77**, 235110 (2008)
29. A.V. Syuy, N.V. Sidorov, A.Y. Gaponov, V.I. Panfilov, M.N. Palatnikov, Opt. Spectrosc. **114** (5), 845 (2013)
30. A.V. Syuy, N.V. Sidorov, A.Y. Gaponov, M.N. Palatnikov, V.G. Efremenko, Optik **124**, 5259 (2013)
31. A.V. Syui, N.V. Sidorov, M.N. Palatnikov, D.S. Shtarev, E.A. Antonycheva, A.Y. Gaponov, K.A. Chekchonin, Opt. J. **82**(5), 71 (2015)
32. N.V. Sidorov, O.Y. Picoul, A.A. Kruk, N.A. Teplyakova, A.A. Yanichev, M.N. Palatnikov, Opt. Spectrosc. **118**(2), 273 (2015)
33. N.V. Sidorov, O.Y. Picoul, N.A. Teplyakova, A.A. Kruk, M.N. Palatnikov, *Perspekt. Mater.* (4), 70 (2014) (in Russian)
34. O.Y. Pikoul, N.V. Sidorov, M.N. Palatnikov, O.V. Makarova, *J. Mod. Phys.* (4), 12 (2013)
35. I.S. Akhmadullin, V.A. Golenishchev-Kutuzov, S.A. Migachev, S.P. Mironov, Fiz.Tverd. Tela **40**(7), 1307 (1998)
36. I.F. Kanaev, V.K. Malinovsky, DAN USSR **266**(6), 137 (1982)
37. N.V. Sidorov, A.A. Gabain, A.A. Yanichev, I.N. Efremov, I.V. Biryukova, M.N. Palatnikov, Opt. Spectrosc. **118**(2), 283 (2015)
38. N.V. Sidorov, M.N. Palatnikov, A.A. Kruk, A.A. Yanichev, O.V. Makarova, N.A. Teplyakova, O.Y. Pikoul, Opt. Spectrosc. **116**(2), 298 (2014)
39. M.N. Palatnikov, I.V. Biryukova, O.B. Shcherbina, N.V. Sidorov, O.V. Makarova, N.A. Teplyakova, Kristallographija **61**(6), 999 (2016)
40. F. Jermann, M. Simon, E. Krätzig, *J. Opt. Soc. Am.* (12), 2066 (1995)
41. N.A. Teplyakova, N.V. Sidorov, M.N. Palatnikov, A.V. Syuy, D.S. Shtarev, Inorg. Mater. **53**(11), 1189 (2017)